Tomographic imaging and scanning thermal microscopy: thermal impedance tomography

R Smallwood[1], P Metherall[1], D Hose[1], M Delves[2], H Pollock[3], A Hammiche[3], C Hodges[3], V Mathot[4], P Willcocks[5]

[1] Medical Physics & Engineering, University of Sheffield, Royal Hallamshire Hospital, Sheffield S10 2JF, UK; [2] NASoftware Ltd, Roscoe House, 62 Roscoe Street, Liverpool L1 9DW, UK; [3] School of Physics and Chemistry, Lancaster University, Lancaster LA1 4YB, UK; [4] Morphology and Colloid Chemistry Department, DSM Research, PO Box 18, 6160 MD Geleen, The Netherlands; [5] ICI Technology – Science Support Group, PO Box 90, Wilton, Middlesborough, TS90 8JE, UK

Abstract

The application of tomographic imaging techniques developed for medical applications to the data provided by the scanning thermal microscope will give access to true three-dimensional information on the thermal properties of materials on a μm length scale. In principle, the technique involves calculating and inverting a sensitivity matrix for a uniform isotropic material, collecting ordered data at several modulation frequencies, and multiplying the inverse of the matrix with the data vector. In practice, inversion of the matrix in impractical, and a novel iterative technique is used. Examples from both simulated and real data are given.

Keywords: scanning thermal microscopy; tomographic imaging; sensitivity matrix; polymers

Introduction

The Scanning Thermal Microscope (SThM) can sense the thermal properties of materials on a sub-μm length scale [1] by applying a constant power input to the material, and measuring the resulting temperature change. The resulting two-dimensional image is a weighted projection of the properties of the bulk material onto the surface plane across which the probe is scanned. If a sinusoidal modulation is applied to the heat input, an evanescent thermal wave is generated which decays exponentially with a thermal diffusion length that depends on the thermal properties of the material, and on the modulation frequency. In principle, therefore, it is possible to access the thermal properties at different depths within the material by varying the modulation frequency. In practice, generating quantitative data related to depth is non-trivial [2].

An analogous problem has been solved for Electrical Impedance Tomography (EIT), a method of generating three dimensional images of the electrical impedance of a material. The particular case that has been solved is for 3D imaging of the human chest [3]. The problem is to reconstruct some property of the interior of a material when measurements are confined to the surface. The starting point is to consider the material to be composed of volume elements (voxels), each of which is assumed to be uniform and isotropic. Measurements can be made at points on the surface – in general, a measurement consists of injecting energy (electrical current, heat) and measuring the resulting change (voltage, temperature). At least one independent measurement has to be made for each voxel. A sensitivity matrix is constructed by calculating the change in the measured property, for every measurement site, of an incremental change in the properties of each voxel. We then have, for the temperature case:

[surface temperature distribution] = [sensitivity matrix] x [distribution of thermal properties]

where [ ] indicates a matrix. The scanning thermal microscope injects heat, and measures the resultant temperature change, with the same probe, so for a volume consisting of l layers and m x n surface points (i.e. l x m x n voxels), only m x n independent measurements can be made. However, we can make measurements at an arbitrary number of modulation frequencies, so a minimum of l modulation frequencies will give sufficient independent measurements.

It is clear that pre-multiplication of the above equation by the inverse of the sensitivity matrix will give:

$$[\text{sensitivity matrix}]^{-1} \times [\text{surface temperature distribution}] = [\text{distribution of thermal properties}]$$

so we can now determine the distribution of thermal properties. We will now show:

1. how the sensitivity matrix is calculated in 1D and 3D (the 1D is relevant for materials consisting of uniform layers)
2. how the computational problem of finding an inverse for the sensitivity matrix is solved
3. results from simulated 1D and 3D data
4. results from real data.

Background Theory

Thermal Diffusion.

The rate at which heat is transferred across a surface per unit area per unit time is the heat flux f. For an isotropic solid, the flux is related to the rate of change of temperature T along the normal to an isothermal by the heat conduction equation:

$$f_n = -k\frac{\partial T}{\partial n} \qquad 1$$

where k is the thermal conductivity, and $\partial/\partial n$ denotes the spatial differential, normal to the isothermal surface.

Consider an element of volume through which heat is flowing but which does not contain any internal sources of heat. For the non-steady case, the possibility of heat storage within the element must be considered and the rate of heat gain in the element from flow across its faces must be equal to the rate of heat storage. This is governed by the rate of temperature change with time and the material properties, density and specific heat. For a homogenous isotropic solid whose thermal conductivity is independent of the temperature, this leads to the diffusion equation:

$$\frac{\partial^2 T}{\partial x}+\frac{\partial^2 T}{\partial y}+\frac{\partial^2 T}{\partial z} = \frac{1}{\alpha}\frac{\partial T}{\partial t} \qquad 2$$

where $\alpha = k/\rho c$ is the diffusivity of the material, ρ the density, and c the specific heat.

If we consider a semi-infinite sample ($T \to 0$ as $z \to \infty$) heated with sinusoidally modulated energy which is absorbed evenly across the entire sample surface ($z = 0$), equation 2 can be considered to be one dimensional, and has the general solution:

$$\begin{aligned} T(z,t) = &\left[e^{\mu z}\left(A\cos(\mu z)+B\sin(\mu z)\right)+e^{-\mu z}\left(C\cos(\mu z)+D\sin(\mu z)\right)\right]\cos(\omega t) \\ &+\left[e^{\mu z}\left(-A\sin(\mu z)+B\cos(\mu z)\right)+e^{-\mu z}\left(C\sin(\mu z)-D\cos(\mu z)\right)\right]\sin(\omega t) \end{aligned} \qquad 3$$

$$\textit{where} \quad \mu = \left(\frac{\omega}{2\alpha}\right)^{1/2} \qquad \omega = 2\pi f \qquad (f = \textit{frequency of applied heat})$$

In figure 1, the temperature profile with depth is plotted for a typical polymer at regular time intervals during a single cycle of the modulated heat input (at 1kHz). We can see that equation 3 can be interpreted as an exponentially damped plane wave propagating in the z direction, with wavelength:

$$\lambda_1 = 2\pi\sqrt{\frac{2\alpha}{\omega}} \qquad 4$$

The damping of the thermal wave is frequency dependent and can be described in terms of the thermal diffusion length μ. This is defined as the distance at which the amplitude has decayed to $1/e$ of the surface value:

$$\mu \equiv \sqrt{\frac{2\alpha}{\omega}} = \lambda_1/2\pi \qquad 5$$

At 1 kHz, for the material in Figure 1, λ_1 = 37 μm.

Insert figure 1

.

By varying the modulation frequency, we can effectively select the penetration depth of the thermal wave and thus interrogate the sample material to progressively deeper levels. In figure 2, the exponential envelope has been plotted for the same polymer over a frequency range from 0.1Hz to 1MHz. In each case, the temperature curve has been normalised to the surface temperature.

Insert figure 2

Now consider the heterogeneous 1-d case in which a discrete perturbation in the material properties is located at depth. For example, consider a material with the same substrate polymer as in figures 1 and 2, but with a perturbation located at depth 2μm to 4μm from the surface. The perturbation corresponds to a 5 fold increase in thermal conductivity but with no change in diffusivity. In figure 3, the temperature profiles for this heterogeneous sample are plotted as in figure 1 (The profiles for the equivalent homogenous material are also plotted for comparison).

Insert figure 3

The buried perturbation clearly alters the temperature profiles from the uniform case, and the depth of the perturbation can be visually identified. In practice however, we are not able to explicitly measure these thermal profiles as measurements can only be made at the surface where the heat is applied. From figure 3 we can see that there is a significant change in signal amplitude at this surface and we note that there is also change in the phase between the applied heat flux and measured temperature modulation compared to the homogenous case.

1D solution with heat losses

In SThM, the 1D solution in equation 3 is of limited practical use as the heat source does not satisfy the semi-infinite criteria of heating the entire surface plane i.e. the source dimensions are not large compared to the wavelength. Hammiche et al. [2], accounted for the finite sized heat source by extending the simple 1D solution to incorporate heat loss from the edges of the 1D sample. Only the zero frequency case was considered and hence no depth information could be obtained. We now generalise this result. The non-steady state 1D differential equation with heat loss h can be written:

$$\frac{\partial^2 T}{\partial z^2} = \frac{1}{\alpha}\frac{\partial T}{\partial t} - hT \qquad 6$$

where $h = \dfrac{\varepsilon p}{kA}$

ε = heat loss coefficient
p = perimeter of elemental heat source
k = thermal conductivity
A = crosssectional area of elemental heat source

which has the general solution:

$$\begin{aligned} T(z,t) = &\left[e^{\mu_1 z}\left(A\cos(\mu_2 z) + B\sin(\mu_2 z)\right) + e^{-\mu_1 z}\left(C\cos(\mu_2 z) + D\sin(\mu_2 z)\right)\right]\cos(\omega t) \\ &+ \left[e^{\mu_1 z}\left(-A\sin(\mu_2 z) + B\cos(\mu_2 z)\right) + e^{-\mu_1 z}\left(C\sin(\mu_2 z) - D\cos(\mu_2 z)\right)\right]\sin(\omega t) \end{aligned} \qquad 7$$

where:

$$\mu_1 = \sqrt{\frac{h+r}{2}}$$
$$\mu_2 = \sqrt{\frac{h-r}{2}}$$
$$r = \sqrt{h^2 + (\omega/\alpha)^2}$$

For the 1D model, the diffusion length was related only to the diffusivity of the sample and the modulation frequency (equation 5). Introduction of the heat loss term indicates that the diffusion length is also be related to the geometry of the probe:

$$\lambda = \sqrt{\frac{2}{r+h}} \quad \text{(as } r \text{ and } h \text{ both contain the perimeter length)} \qquad 8$$

3D solution with heat losses

An analytical solution for a heterogeneous 3D sample is generally not possible, so a Finite Element Model approach using a customised solver has been used. The sample will be effectively semi-infinite on the scale of probe size and solution space, which is of the order of μm. To solve the forward problem the FEM must model the semi-infinite domain with sufficient accuracy such that the finite boundary of the model does not introduce significant errors. Infinite elements [4] are the simplest and most elegant solution, and surround the finite elements on all but one surface, this being the measurement plane. It is assumed that this measurement surface is thermally insulated and heat can only pass into the medium at the probe contact. In this work the core finite elements are isotropic 8 node bricks and the infinite elements also have 8 nodes and only one infinite surface.

To simulate a variety of probe sizes, distributed loads have been used in the form of square arrays containing a number of load points. The amplitude of the applied heat flux at each node is determined by assuming the probe is made up of smaller probes which cover only a single element and the same heat flux is applied through each of the 4 corner nodes. As these smaller probes intersect at common nodes, the overall applied heat flux is found by summing the contributions of these smaller probes. A 4x4μm probe is simulated using an array of 25 nodes.

To investigate the thermal diffusion length limit we need to perform an analysis at a modulation frequency such that $\lambda_f \approx \lambda_{f=0}$. If we plot the normalised temperature of the nodes beneath the centre of the probe array at various time intervals in the modulation cycle, we can examine the temperature profile with depth and determine the thermal diffusion lengths. Figure 4 shows the temperature profiles for probes varying in size from 1x1 μm to 12x12 μm.

Insert figure 4

In each case the applied modulation frequency was 0.1 Hz, but checks were performed to ensure that the limit had been reached. The plots clearly show that increasing the probe size results in a deeper penetration of the thermal wave and thus a correspondingly increased sensitivity at these deeper planes. The two plots for the 1x1 μm probe (figure 4a & 4b), suggests that in 3D, the diffusion length is independent of the thermal properties of the material. This is in contrast to 1D models as indicated in equation 4.

We need to characterise the situation that involves both temperature modulation and three-dimensional heat flow. For this purpose we define an effective diffusion length λ_ω, and it proves possible to express this in terms of two other characteristic lengths, one of which is λ_1 as defined in equ. (4). The other is a "zero-frequency diffusion length", λ_0: consider the limiting case of equation (8) as the frequency is reduced to zero. The diffusion length for the lossy system then becomes:

$$\lambda_0 \rightarrow h^{-1/2} \qquad 9$$

Thus even with no modulation, the temperature in the medium falls rapidly with distance from the source, with λ_0 being governed by the size of the probe. Furthermore, as we have seen from the finite element analyses, λ_0 is almost independent of the thermal properties of the medium!

The three-dimensional finite element analysis leads to the following simple relation:

$$\lambda_\omega^2 \times ([\lambda_0^{-4}+4\,\lambda_1^{-4}]^{1/2}+ \lambda_0^{-2}) = 2 \qquad 10$$

Of course, λ_0 is generally less than λ_1, and if $\lambda_0 << \lambda_1$ then we can use the binomial approximation to derive the extremely simple approximation –

$$\lambda_\omega \cong \lambda_0 \times [1- 0.5(\lambda_0 /\lambda_1)^4] \qquad 11$$

This implies that we can consider the effect of frequency as lying within one of four "domains":

Low frequency (large λ_1, small λ_0): no significant effect of frequency upon λ_ω, which tends towards λ_0. Depending on the sample material, if we want frequency discrimination it may be necessary to use a probe of large diameter. There will therefore be a trade off between the increased scan depth and a reduced planar spatial resolution due to the required larger probe size. For this linear problem, a large probe can be synthesised from a number of measurements by a smaller probe;

(b) Moderate frequency: λ_ω is given by the simple binomial approximation;

(c) High frequency: the exact equ. is needed;

(c) Very high frequency (very small λ_1, very large λ_0): here, another binomial approximation applied to the exact equation gives –

$$\lambda_\omega \cong \lambda_1 \times [1- (\lambda_1 /2\lambda_0)^2] \qquad 12$$

tending towards λ_1 if either the modulation frequency, or the probe size (and λ_0), is very large.

Sensitivity matrix

For a given change in thermal properties $\Delta k = k_p - k_r$ (where subscripts *p* and *r* refer to the perturbed and reference cases respectively), there will be an associated change in the measured surface temperature amplitude $\Delta T = T_p - T_r$. There will also be an associated change in the phase between the applied heat flux and the temperature, but we shall only consider the variation in amplitude due to the practical difficulties of making accurate phase measurements.

The ratio of these quantities is defined as the sensitivity:

$$s = \frac{\Delta T}{\Delta k} \qquad 13$$

The sensitivity will vary with the depth of the material perturbation and with modulation frequency. If we assume that there is a linear sensitivity relationship, then the sensitivity relationship for each measurement frequency f can be represented by a set of linear equations:

$$\Delta T_f = s_{f,i} \Delta k_i \qquad 14$$

which can be written in matrix notation as:

$$\mathbf{t} = \mathbf{S}\mathbf{k} \qquad 15$$

Here $\mathbf{t}$ is the vector of the change in surface temperature at each measurement frequency, $\mathbf{k}$ is the change in thermal properties in each of the discrete elements and $\mathbf{S}$ is the sensitivity matrix. Perturbing each element in turn and finding the corresponding sensitivity coefficient for each of the measurement frequencies forms the sensitivity matrix. As we perturb the deeper regions in the material, the temperature change will gradually reduce until it is at such a level that it can not be measured above the unavoidable measurement noise.

Matrix inversion: solving the inverse problem

To recover the spatially distributed material properties Δk_i from the measured surface measurements ΔT_f we have to solve:

$$\mathbf{k} = \mathbf{S}^{-1}\mathbf{t} \qquad 16$$

In general a large change in **k** will usually result in only a small change in **t** and these measurements are said to be ill-posed, i.e. many of the elements of the sensitivity matrix are very close to zero. The sensitivity matrix is therefore highly ill-conditioned and the true matrix inverse does not exist. In Electrical Impedance Tomography, truncated singular value decomposition (SVD) was used in order to assess the degree of matrix condition, perform the regularisation, and find its pseudo-inverse [3]. As a rule of thumb, the level at which the singular values are truncated is at a level which corresponds to the measurement signal to noise ratio. Solution techniques must take the following factors into account:

1. The matrix **S** may not be square: in the EIT case the solution grid is finer than the measurement grid ("super-resolution") and the set of equations is then underdetermined.
2. Even when **S** is square the matrix is *very ill-conditioned*: the reconstruction process is ill-posed.

This is a standard approach which works well in applications (such as EIT) for which the singular value spectrum has a pronounced knee so that choosing a suitable cutoff can be done. However, the primary disadvantage of the pseudo-inverse technique is that its computation does not scale well: the cost of a straightforward implementation of the technique is proportional to the cube of the number of unknowns, and for the thermal problem this leads to estimates of 6 Tbytes of storage and 2000 years to invert the matrix!

It is not logically necessary to produce a full singular value decomposition of **S**. Once the cutoff value has been chosen, and experiments made to determine how many singular values (say M) are likely to fall above this cutoff, then only the largest M singular vector/value triplets are needed. Standard algorithms exist for this; but these still require the full sensitivity matrix **S**. However, **S** is highly structured. An iterative technique was developed for computing the M largest singular triplets which needed only values of **Sv** (and **S'v**) for a vector **v**; these matrix-vector products can be computed without forming **S**. Since the partial SVD decomposition can be carried out offline (it depends only upon **S**, not upon the sample measurements **t**) the time taken for a given **k** is also low.

The Best Linear Estimate Technique

The SVD reconstruction technique itself is less effective than for the EIT problem, because the SVD spectrum has no sharp knee. An algorithm based on the Best Linear Estimate (BLE) method has therefore been used to solve the inverse problem. The BLE or Stochastic Inverse algorithm addresses the illconditioning by explicitly considering the inaccuracies in the measurement of the vector **t**, treating these inaccuracies as noise. It addresses the equations:

$$\mathbf{Sk} = \mathbf{t} + \mathbf{n} \qquad 17$$

where **n** represents the noise and is supposed random; and seeks the "best" (in a stochastic least squares sense) linear reconstruction of **k**. This yields the defining equations:

$$(\mathbf{SWS}' + m\mathbf{I})\mathbf{k} = \mathbf{t} \qquad 18$$

where **W** is a matrix which itself depends upon **k**, and m is related to the estimated noise level and **I** is the identity matrix.

W represents the expected value of $\mathbf{k}^2$ taken over all noise instantiations. Estimating **W** requires a "world model": prior knowledge of the class of solutions sought. This is the major advantage of the BLE approach: the technique can be tailored to the specific application. Given a world model and an estimate of the noise in the measured response, an iterative search technique is used to produce a solution to the original problem which is a best fit in a linear sense to this model.

Computationally we considered three cases: 1) small occlusions in the sample; 2) layered samples based on a large grid; and 3) a 1-D layered system where the layers are seen as single entries in the solution vector. This system stems from the physical model in which the measurement probe is effectively infinite in size. Cases 1 and 2 generate very large computational problems and differ in the

world model appropriate to the solution. Case 3 has the same world model as Case 2, but is computationally very much simpler.

The sensitivity matrix is large for the 3-D formulation. The size is $\left(n_x \times n_y \times n_d\right) \times \left(n_x \times n_y \times n_f\right)$ where n_x is the grid size in the x direction, n_y the grid size in y direction, n_d the grid size in depth, and n_f the number of modulation frequencies. For a 32x32x8 grid with 8 frequencies, the matrix size is $2^{26} \approx 67.10^6$ elements. The structure of the matrix was exploited in order to reduce the time taken to solve the problem. The problem was formulated using the SVD decomposition of the sensitivity matrix. The full SVD decomposition is not available due to its expense in both time and memory but about 500 of the largest SVD values were generated. The matrix has a double Block Toeplitz structure with only $\left(n_x \times n_y \times n_d \times n_f\right)$ distinct elements. By exploiting the structure of Toeplitz matrices the matrix vector multiplications can be performed at FFT speed.

Experimental

Comparison of SVD and BLE with model data

The Singular Value Decomposition and Best Linear Estimator methods were compared for a solution space (8x8x8 cubic voxels of side 1μm) which was sufficiently small that SVD inversion of the sensitivity matrix was feasible. Data vectors for 8 modulation frequencies were calculated for a uniform isotropic medium ($k=0.142\ Wm^{-1}K^{-1}$, $\alpha=0.11x10^{-6}\ m^2s^{-1}$) containing two 2μm sided cubic inclusions which represent a 100% change in thermal conductivity. These were positioned at different depths. To avoid inverse-crimes[5] a slightly larger model was used to compute the simulated data sets compared to that used to generate the sensitivity matrix. Figure 5 shows a comparison between the two reconstruction methods. The problem with the small 1x1μm probe is demonstrated when multiple inclusions are reconstructed as the signal from the superficial inclusion dominates signals from deeper planes. However, as the probe size is increased to 12x12μm, the true extent of the superficial inclusion is found and the deeper inclusion can be detected. The improvement in image sharpness with the BLE reconstruction is self-evident.

Insert figure 5

BLE reconstruction with 1D (layered) samples

In scanning thermal microscopy, a modulated heat input is applied to the sample at frequency ω and the 3rd harmonic temperature response is measured at the surface (see 3ω method [6] in appendix). The probe is scanned across the sample in a raster fashion so that a 2-d image can be formed as shown in Figure 6. By applying the heat over an range of increasing modulation frequencies the penetration depth of thermal wave progressively shortens. In this way it is possible to obtain 3-d information regarding the sub-surface features in a non-destructive way.

Insert figure 6

Initial efforts have concentrated on the reconstruction of real samples with layered structures (effectively 1D) as considerable difficulties were met in the fabrication of 3D test samples with known morphology Several suitable samples have been produced by the industrial partners within this consortium. These include:

- Bulk PET (poly(ethylene terephthlate)) [1 mm thick sheet]
- Steel [3 mm thick]
- GLC sample: multilayered film consisting of 5 μm thick PET
  40nm Aluminium
  5μm adhesive
  25μm PET
- 25 μm PET on a steel substrate (500 μm)
- Barrier packaging film #1: The total thickness is 46 μm, The composition is not completely known but it contains polyamide and polyethylene. The thickness' of the six different successive layers are: 3 μm; 0.5 μm; 11 μm; 6,5 μm; 1 μm and 24 μm.
- Barrier packaging film #2: The total thickness is 117 μm. At the outer side is a 17 μm thick layer with a melting point of 255 °C (PET). Then follows a print layer, 3 μm thick. The third layer is an adhesive, 2 μm thick. Layer 4 is 7 μm thick aluminium. Layer 5 is an adhesive with a thickness of 2 μm and a melting point slightly below 70 °C. Layer 6 is at the back of the film. It is PE-grade with a thickness of 86 μm and it has a melting point of 112 °C.

Cross-sectional images of the barrier packaging films are shown in Figure 7. Small pieces of both films have been embedded in epoxy resin and then thin slices perpendicular to the film have been cut by means of a microtome. The slices are photographed in transmitted light on a microscope to show the different layers of the film. They are both examples of 'high-tech films' which are routinely dealt with by the end user community.

Insert figure 7

Data has been collected from these samples using AC SThM over the modulation frequency range 10Hz to 10kHz. Measurements were carried out using purpose-built electronic instrumentation together with an EG&G lock-in amplifier model 5302 with 1 MHz bandwidth and n^{th} harmonic (including 3^{rd} harmonic) detection capability. Positioning of the probe on the surface sample with constant force feedback was carried out using a ThermoMicroscopes Explorer AFM. A Wollaston wire resistive thermal probe was used as a highly localised heat source, so as to apply a modulated temperature program to the surface of the sample at the contact point. Based on calibration using the melting points of a number of polymers, the amplitude modulation of the temperature is estimated at 10 K. Probe current is modulated at frequency ω. The voltage across the probe, at the third harmonic frequency 3ω, is monitored by the lock-in amplifier. A Visual Basic program, using ThermoMicroscopes 'SPMTools' routines, was written to ramp up the frequency automatically, and to log data through the microscope controller. As these samples are layered structures, it is appropriate to collected the data at only a single point and use the 1D (lossy) reconstruction. In Figure 8, the raw temperature amplitude data is plotted which shows that the different samples give quite different frequency responses. It is these differences which facilitate the subsurface imaging. It is interesting to note that the PET on steel sample gives an almost identical response to bulk PET. This suggests that the 25μm PET layer is too thick for the steel to be detected below and gives an indication as to the maximum scanning depth for this probe size. It is also of interest that overall, both the packaging films give a lower temperature amplitude than the bulk steel sample.

Insert figure 8

Using these data sets, we can normalise them to a reference. For example we can normalise the GCL sample (which is largely PET with a 40nm layer of aluminium and 5μm adhesive layer) to the bulk PET sample. The reconstructed image should then indicate the percentage change in thermal conductivity of the GCL sample referenced to PET. In order to validate the reconstruction we can

generate simulated data using typical thermal properties of constituent materials. In Figure 9, the real and simulated images have been reconstructed using the BLE method with 128 independent frequency measurements which results in a 128 element 1-d image.

Insert figure 9

The reconstruction of the virtual sample clearly identifies the high conductivity Al layer, but not the adhesive layer immediately below the Al (the thermal properties of this layer were not known). In the reconstruction of the data from the real sample, the high conductivity Al layer is again seen, with a backing layer representing the adhesive. The changes at 14 -19 μm and at > 28 μm are artefacts of the reconstruction method, which decrease as the number of elements in the reconstruction increase. These results show that imaging of layered materials is possible. There are, however, a-priori reasons to suggest that 1-d reconstruction techniques are non-optimal. The sensitivity matrix formulation of the problem contains the implicit assumption that a change in the thermal properties of a single element does not affect the heat flow through the material. This is a reasonable assumption for a 3-d reconstruction of a material with discrete inclusions, but is clearly not a good assumption for a 1-d reconstruction.

In Figure 10, the image reconstruction of the barrier packaging samples are shown. The data has been normalised to reference data which was measured on the underside (substrate side) of the sample. The substrate is sufficiently deep to be considered infinitely thick. In these two cases, a number of layers have been identified within each material, but the limitations of 1-d reconstruction limit the accuracy with which both the position and conductivity of each layer can be estimated.

Insert figure 10

Attempts at obtaining a data set which is suitable for 3D reconstruction is still continuing. Problems have been encountered which are primarily due to the difficulties in fabricating suitable test samples with known morphology. The requirements for a test sample are 1) the surface should be independent of the position of any inclusion (because current scanning thermal microscopes are unable to distinguish between topological changes and thermal changes) and 2) an object or objects of known thermal properties must be placed within the material at a known position. This has proved to be unexpectedly difficult (particularly the surface topography condition), and requires further effort. The latest results can be found on the TASM web-site. http://www.shef.ac.uk/uni/academic/I-M/mpce/tasm

Summary

The scanning thermal microscope measures thermal properties in a plane, which are a non-linear projection of the three-dimensional properties of the material onto the surface. The resulting data is frequency dependent, which gives access to the third dimension. Decoding this data to produce an image of the thermal properties in three dimensions is an extremely large computational problem. The use of iterative methods to solve the inverse problem has been shown to be feasible, but still requires testing with non-layered materials of known morphology.

Appendix: the 3ω method applied to Scanning Thermal Microscopy

Insert figure 11

The heating current is:

$$i = I_0 + I_\omega \cos(\omega t)$$

and the heat flux Q is given by i^2R:

$$Q = \frac{R}{2}\left(2I_0^2 + I_\omega^2 + 4I_0 I_\omega \cos(\omega t) + I_\omega^2 \cos(2\omega t)\right)$$

Assuming the heat flux at these 3 frequencies is constant, this will lead to a surface temperature fluctuation T at the probe

$T = T_0 + T_\omega \cos(\omega t + \phi_\omega) + T_{2\omega} \cos(\omega t + \phi_{2\omega})$. Now R will vary due to this temperature fluctuation as:

$$R = R_0\left[1 + \alpha(T - T_a)\right]$$

where T_a is the ambient temperature (and can be set to zero), and α is the temperature resistivity coefficient for the probe. The voltage across the resistor is given simply as $v = iR$, which in this case is:

$$V = \left[I_0 + I_\omega \cos(\omega t)\right]\left[R\left(1 + \alpha T\right)\right]$$

substituting for T

$$V = R\left[I_0 + I_\omega \cos(\omega t)\right]\left[1 + \alpha\left(T_0 + T_\omega \cos(\omega t + \phi_\omega) + T_{2w} \cos(2_{\omega t} + \phi_{2\omega})\right)\right]$$

$$V = R\left[I_0 + I_0\alpha T_0 + I_0\alpha T_\omega \cos(\omega t + \phi_\omega) + I_0\alpha T_{2\omega} \cos(2\omega t + \phi_{2\omega}) + I_\omega \cos(\omega t) + I_\omega\alpha T_0 \cos(\omega t) + I_\omega\alpha T_\omega \cos(\omega t)\cos(\omega t + \phi_\omega) + I_\omega\alpha T_{2\omega} \cos(\omega t)\cos(2\omega t + \phi_{2\omega})\right]^{e}$$

xpanding and grouping frequency terms gives:

$$V = R\left[I_0\left(1 + \alpha T_0\right) + \frac{1}{2} I_\omega\alpha T_\omega \cos(\phi_\omega) + I_\omega\left(1 + \alpha T_0\right)\cos(\omega t) + I_0\alpha T_\omega \cos(\omega t + \phi_\omega) + \frac{1}{2} I_\omega\alpha T_{2\omega} \cos(\omega t + \phi_{2\omega}) + I_0\alpha T_{2\omega} \cos(2\omega t + \phi_{2\omega}) + \frac{1}{2} I_\omega\alpha T_\omega \cos(2\omega t + \phi_\omega) + \frac{1}{2} I_\omega\alpha T_{2\omega} \cos(3\omega t + \phi_{2\omega})\right]$$

The 2ω component of the measured voltage v will therefore be a complicated combination of the ω and 2ω temperature amplitudes with a corresponding phase combination, given by:

$$V_{2\omega} = K \sin(2\omega t + \phi_\omega + \theta)$$

where

$$K = \sqrt{\left(I_0 R\alpha T_{2\omega} + \frac{1}{2} I_\omega R\alpha T_\omega \cos(\phi_{2\omega} - \phi_\omega)\right)^2 + \left(\frac{1}{2} I_\omega R\alpha T_\omega \sin(\phi_{2\omega} - \phi_\omega)\right)^2}$$

$$\theta = \sin^{-1}\left(\frac{I_\omega R\alpha T_\omega \sin(\phi_{2\omega} - \phi_\omega}{2K}\right)$$

The 3ω signal which gives $T_{2\omega}$ and $\phi_{2\omega}$ directly, measures how the resistance changes with thermal power rather than just input current. Its value is independent of R_0, and thus, independent of errors based on inhomogeneous temperature distributions in sample or probe. However, the signal is relatively weak.

Figure 1. *1D temperature profiles with depth during a cycle of a 1kHz modulated heat input. Material properties: k = 0.142 $Wm^{-1}K^{-1}$, α = 0.11e-6 m^2s^{-1}. In practice a DC offset is applied to that the probe temperature is always above ambient, but this has been ignored for clarity*

Figure 2. *1D temperature profile envelope plotted for the same material as in figure 1 over a range of modulation frequencies (0.1 Hz to 1 MHz). Each profile has been normalised to the surface temperature.*

Figure 3. *1D temperature profiles for an inclusion buried at depth 2μm to 4μm within the substrate as described in figure 1 (also shown). The inclusion corresponds to a 5 fold increase in thermal conductivity compared to the substrate, but with no associated change in thermal diffusivity. The DC offset has been ignored for clarity.*

Figure 4 *Temperature profiles for various sized probes and two homogenous materials at 0.1Hz (mat-1: k=0.142 $Wm^{-1}K^{-1}$, α = 0.11x10^{-6} $m^{-2}s^{-1}$; Mat-2: k=0.0238 $Wm^{-1}K^{-1}$, α = 18.4x10^{-6} $m^{-2}s^{-1}$). a) 1x1μm probe - mat1, b) 1x1μm probe – mat2, c)4x4μm probe - mat1, d)6x6μm probe - mat1, e)8x8μm probe - mat1, f)12x12μm probe - mat1*

Figure 5. *3D reconstruction of computer simulated data sets. The ideal image represents the FEM model thermal distribution from which the simulated data sets are generated. Results for two different probe sizes (i.e. contact area) are given for the SVD and BLE reconstruction methods.*

Figure 6. *Scanning Thermal Microscopy. The probe is scanned with constant force, variations in heat flow out of the probe are measured by monitoring the Wheatstone bridge voltage which is then used to create contrast in the thermal image.*

Figure 7. *'Edge-on' transmitted light micrograph of the barrier (sausage and coffee) packaging film samples. The samples appear curved although the original film is actually flat.*

Figure 8. *Temperature amplitude variation with modulation frequency for the layered samples studied.*

Figure 9. *1-d BLE reconstruction of a simulated and real sample corresponding to the GCL film (5mm PET, 40nm Al, 5μm adhesive, 25μm PET) referenced to bulk PET.*

Figure 10. *1D BLE reconstruction of the barrier packaging samples referenced to the substrate side of each sample.*

Figure 11. *No caption.*

[1] A Majumdar, Scanning Thermal Microscopy, Annu Rev Mater Sci 29 (1999) 505-585.

[2] A Hammiche, H M Pollock, M Song and D J Hourston, Sub-surface imaging by scanning thermal microscopy, Measurement Science & Technology 7 (1996) 142-150

[3] P Metherall, D C Barber, R H Smallwood and B H Brown B H, Three Dimensional Electrical Impedance Tomography, Nature 380 (1996) 509-512

[4] P Bettess, Infinite Elements, Int. J. Num. Meth. Engng, **11** (1977) 53-64

[5] D L Colton and R Kress, Inverse Acoustic and Electromagnetic Scattering Theory. Applied Mathematical Sciences 93: (1992) Springer-Verlag, Berlin.

[6] D G Cahill Thermal conductivity measurement from 30 to 750 K: the 3ω method. Rev Sci Instrum 61 (1990) 802-808

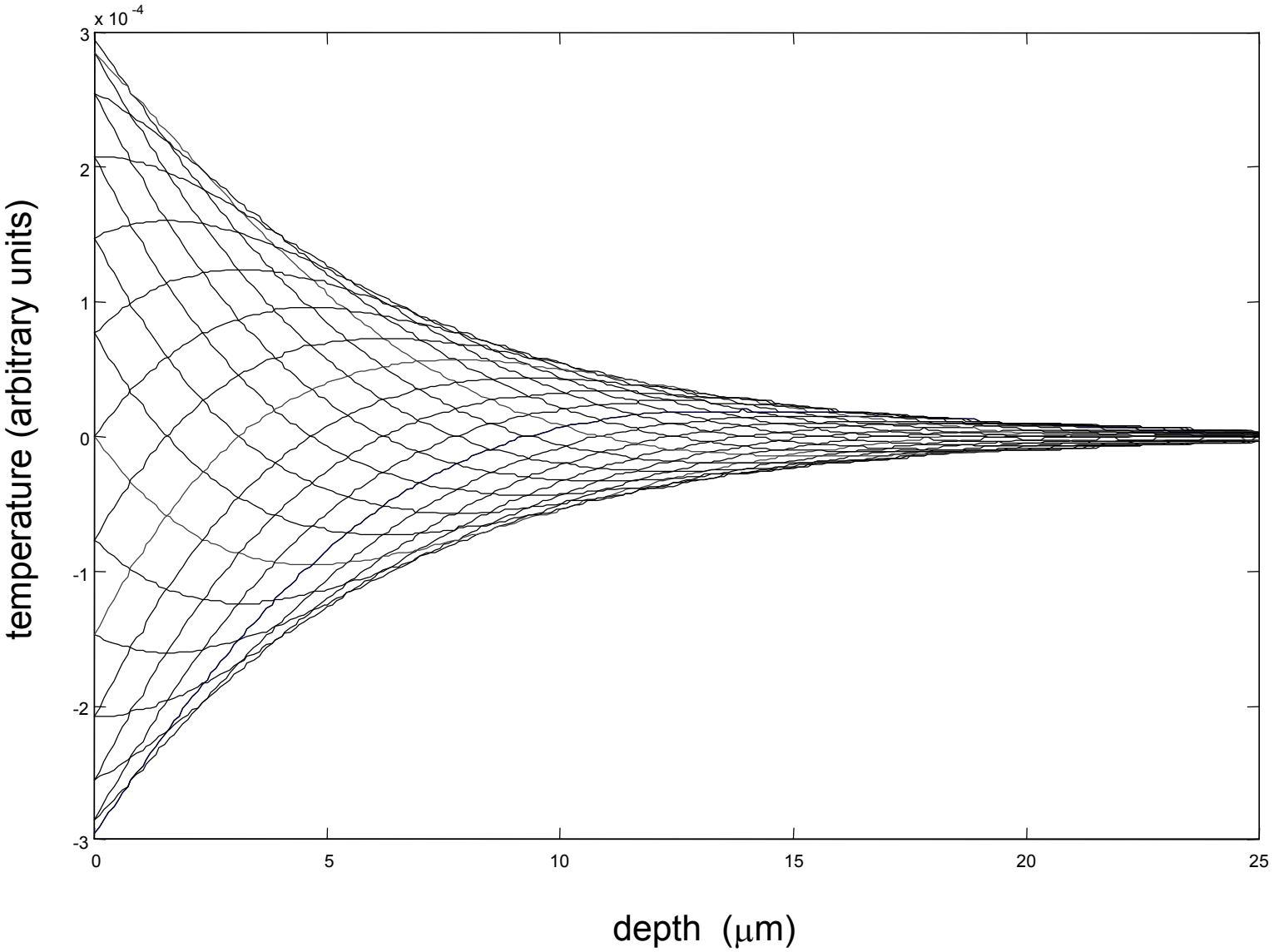
x 10 -4
3
2
1
0
-1
-2
-3
temperature (arbitrary units)
0
5
10
15
20
25
depth (μm)

Figure 1

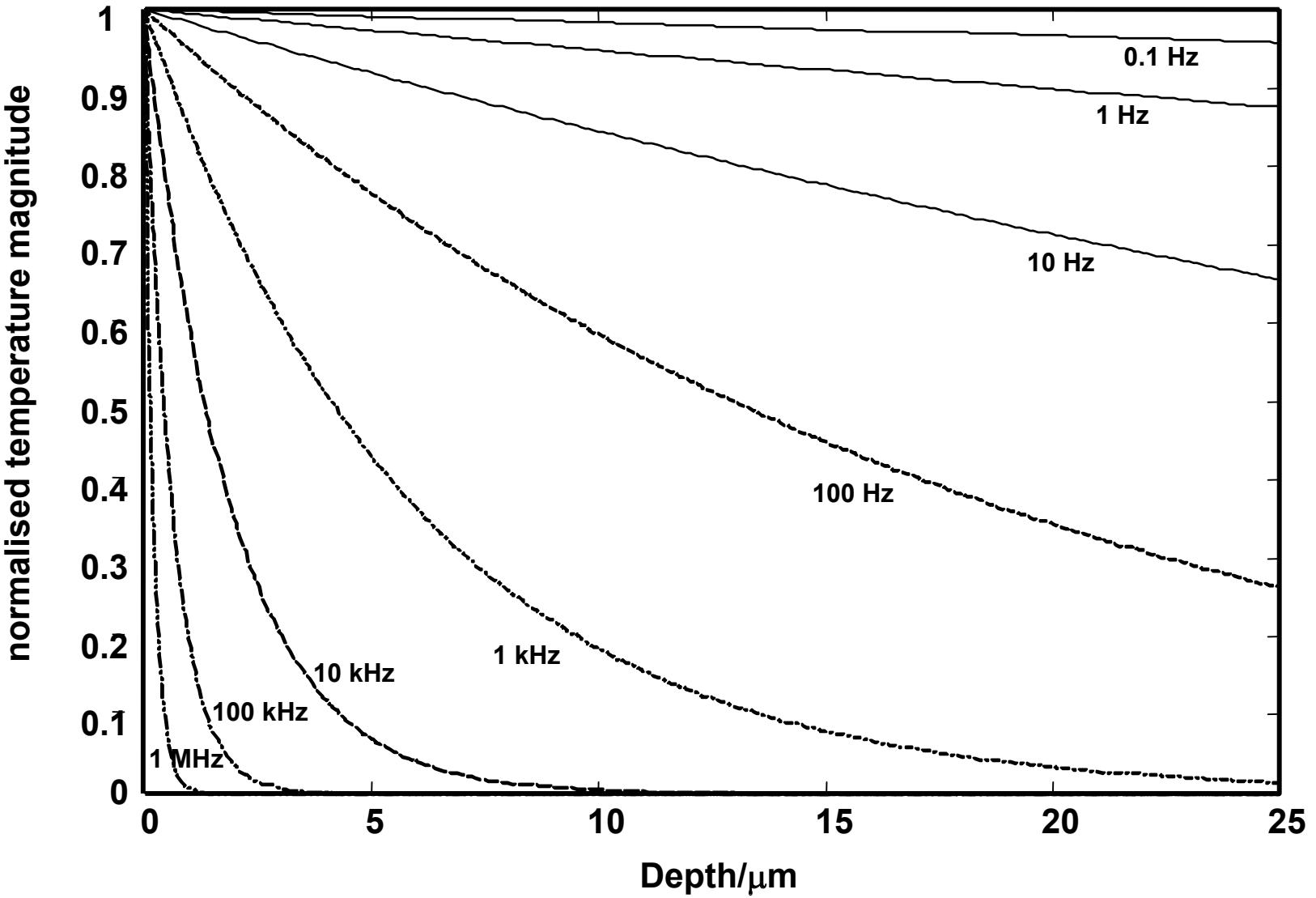
normalised temperature magnitude
1
0.9
0.8
0.7
0.6
0.5
0.4
0.3
0.2
0.1
0
0
5
10
15
20
25
Depth/μm
0.1 Hz
1 Hz
10 Hz
100 Hz
1 kHz
10 kHz
100 kHz
1 MHz

Figure 2

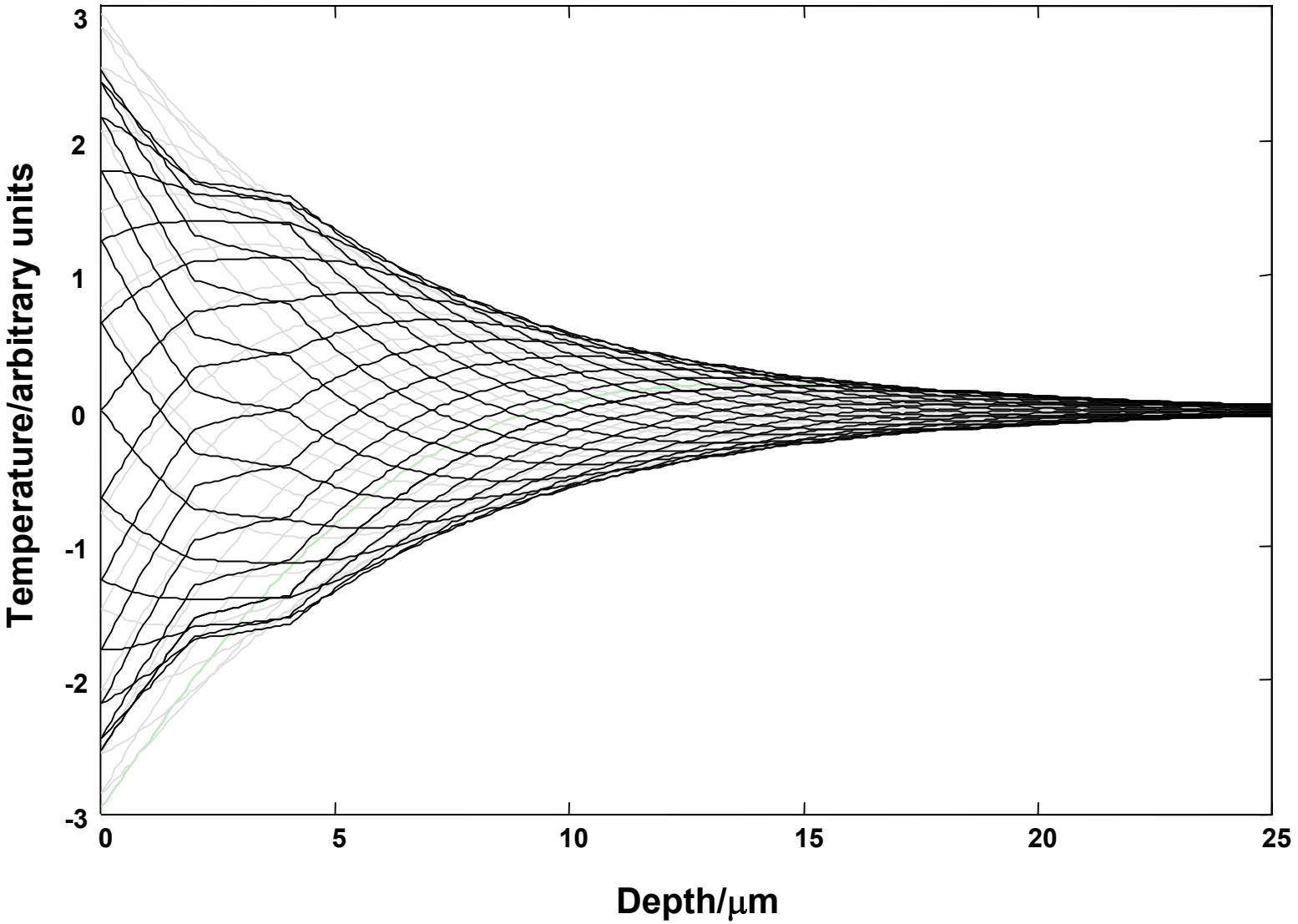

Figure 3

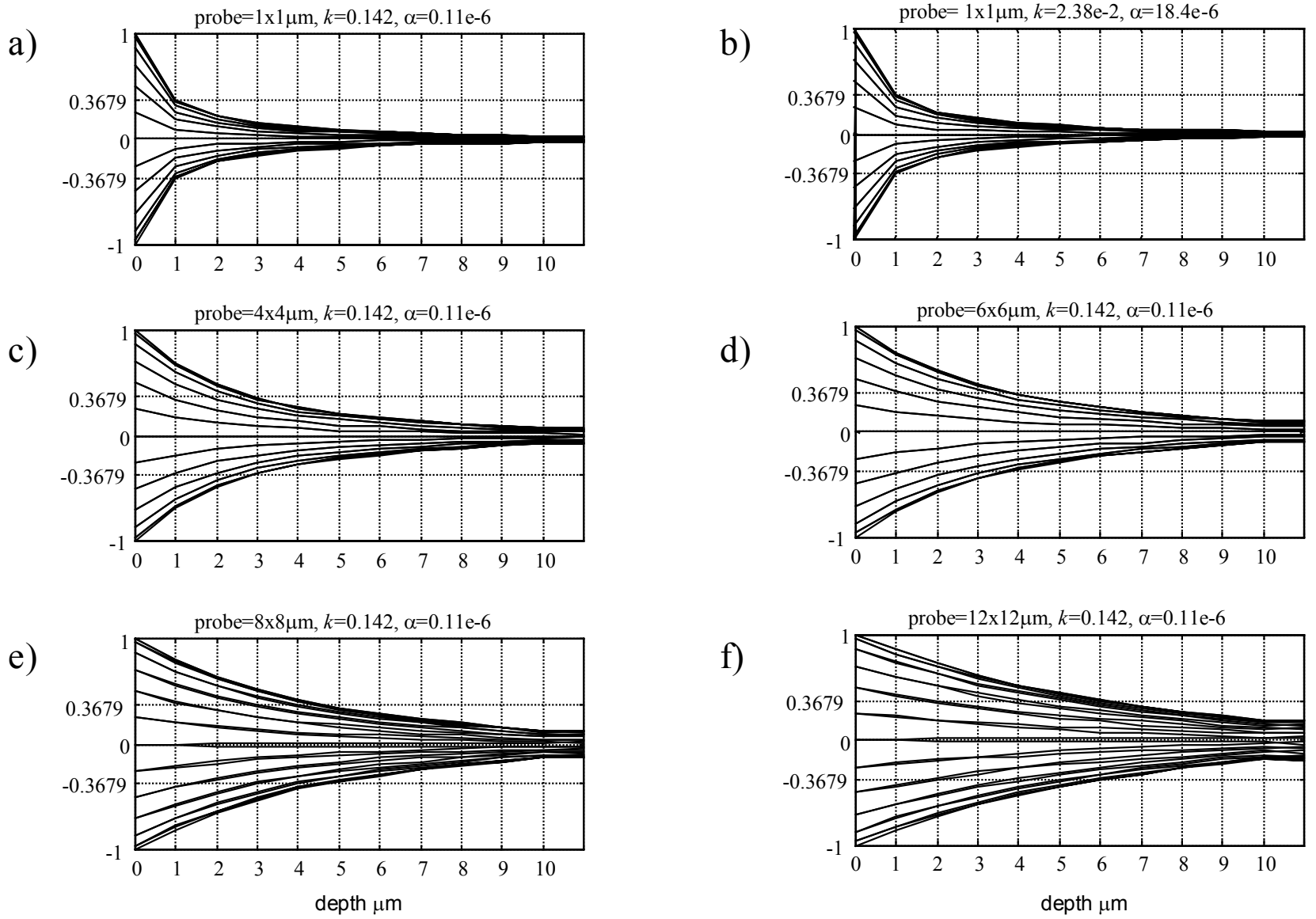
a)
probe=1x1μm, k=0.142, α=0.11e-6
b)
probe= 1x1μm, k=2.38e-2, α=18.4e-6
c)
probe=4x4μm, k=0.142, α=0.11e-6
d)
probe=6x6μm, k=0.142, α=0.11e-6
e)
probe=8x8μm, k=0.142, α=0.11e-6
f)
probe=12x12μm, k=0.142, α=0.11e-6
1
0.3679
0
-0.3679
-1
0 1 2 3 4 5 6 7 8 9 10
depth μm

Figure 4

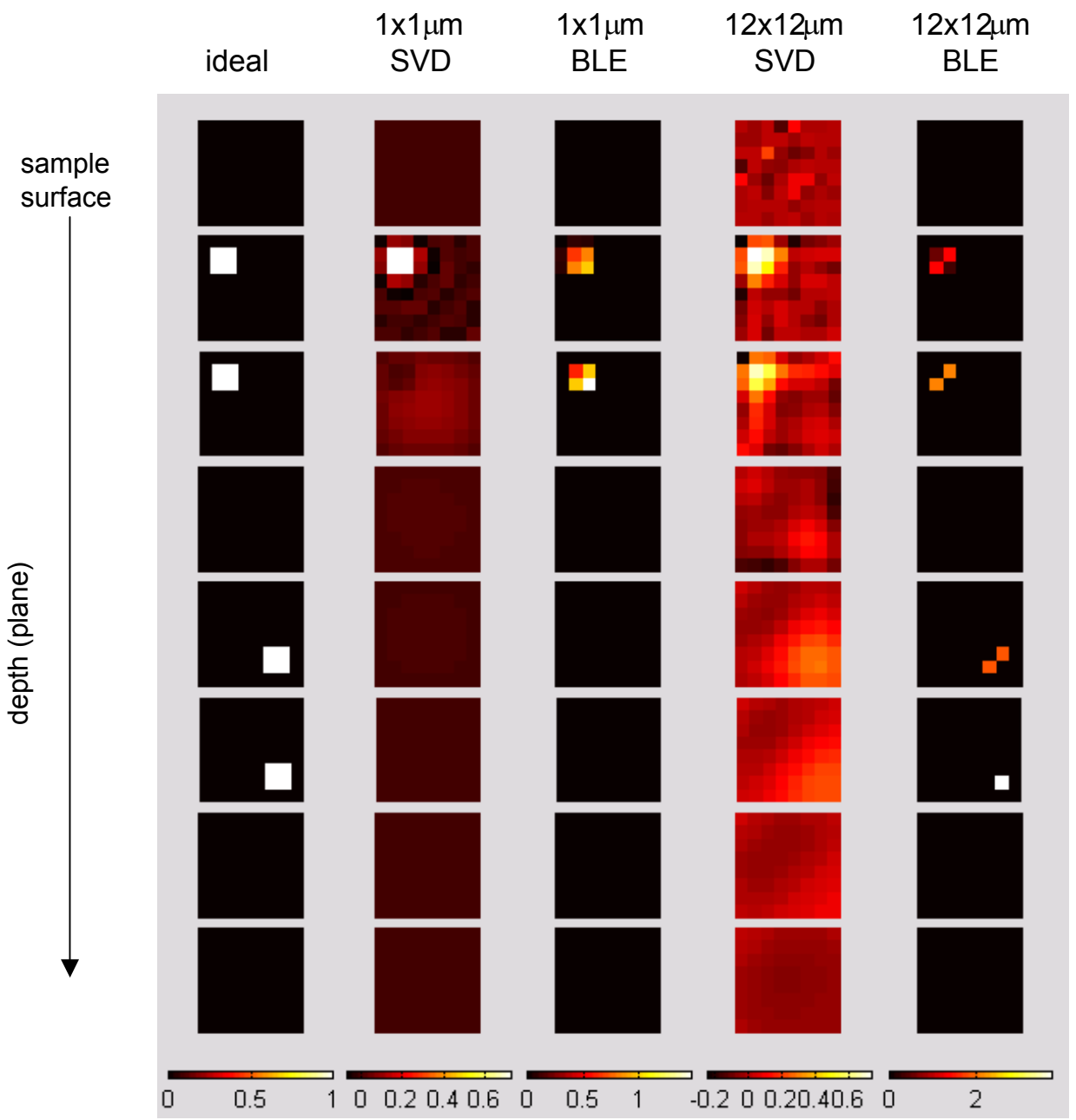
ideal
1x1μm SVD
1x1μm BLE
12x12μm SVD
12x12μm BLE
sample surface
depth (plane)
0 0.5 1
0 0.2 0.4 0.6
0 0.5 1
-0.2 0 0.2 0.4 0.6
0 2

Figure 5

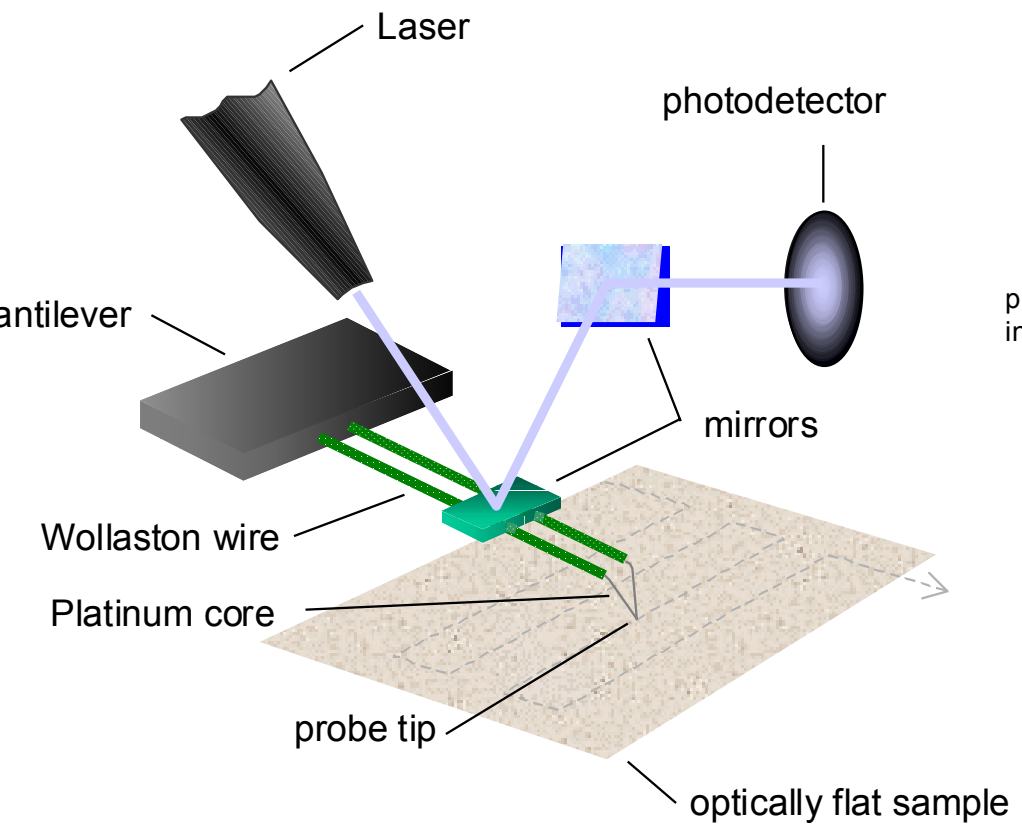

Basic Circuit Operation

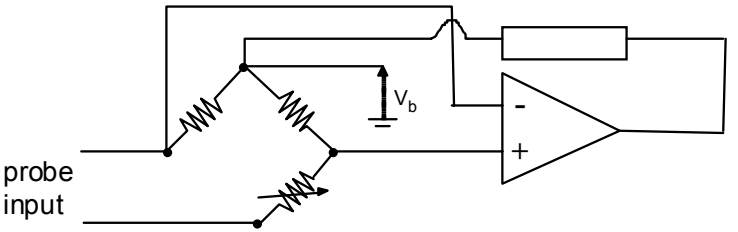

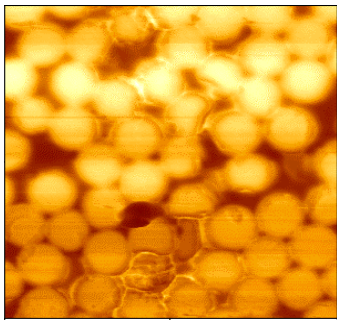

signal V_b can be displayed as a 2-d image

igure 6

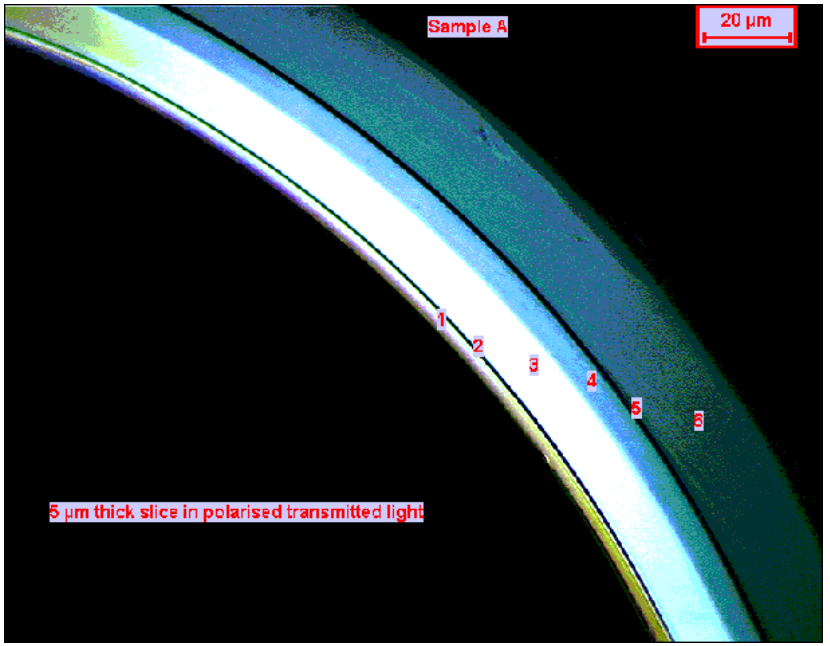

Barrier packaging material #1
(outer surface on the left)

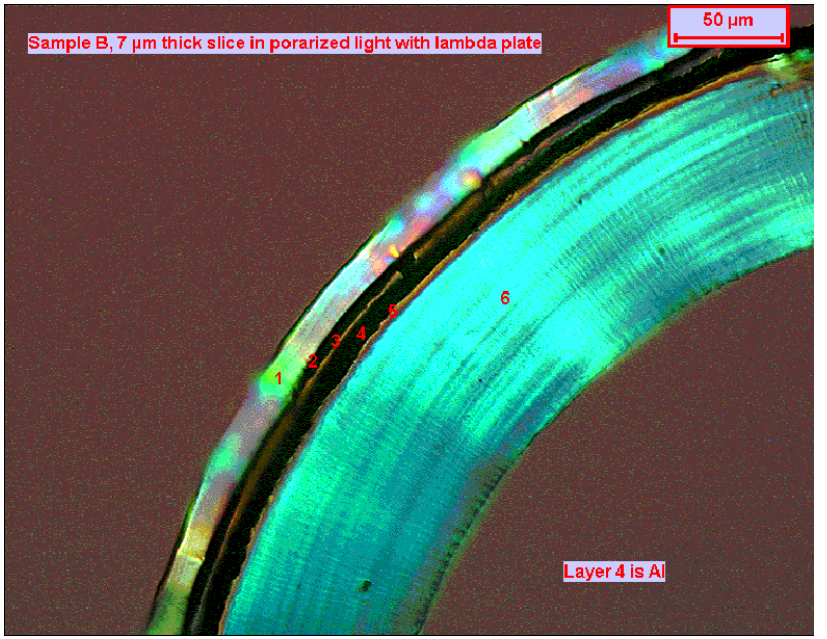

Barrier packaging material #2
(outer surface on the left)

igure 7

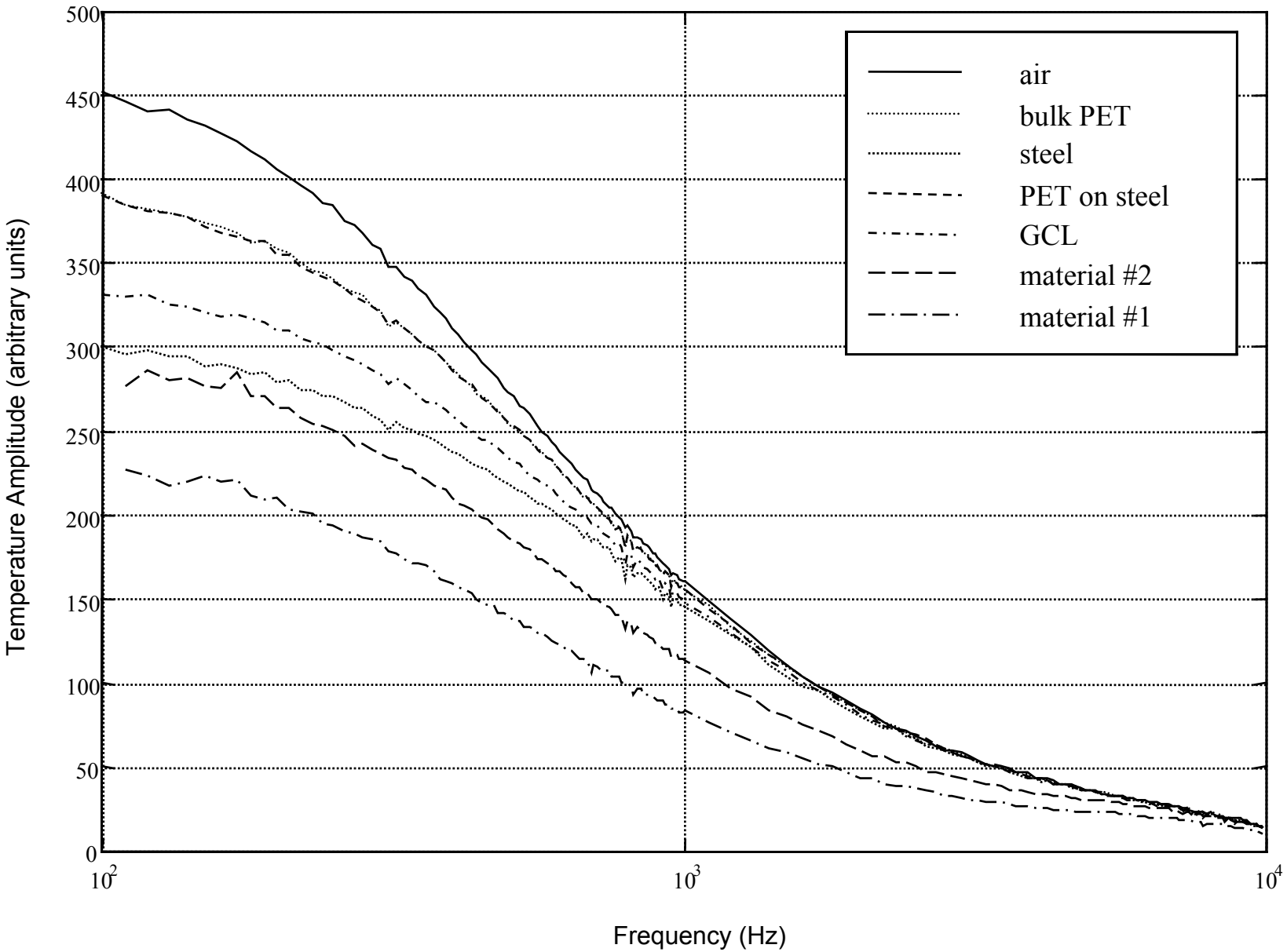
500
450
400
350
300
250
200
150
100
50
0
Temperature Amplitude (arbitrary units)
10^2
10^3
10^4
Frequency (Hz)
air
bulk PET
steel
PET on steel
GCL
material #2
material #1

Figure 8

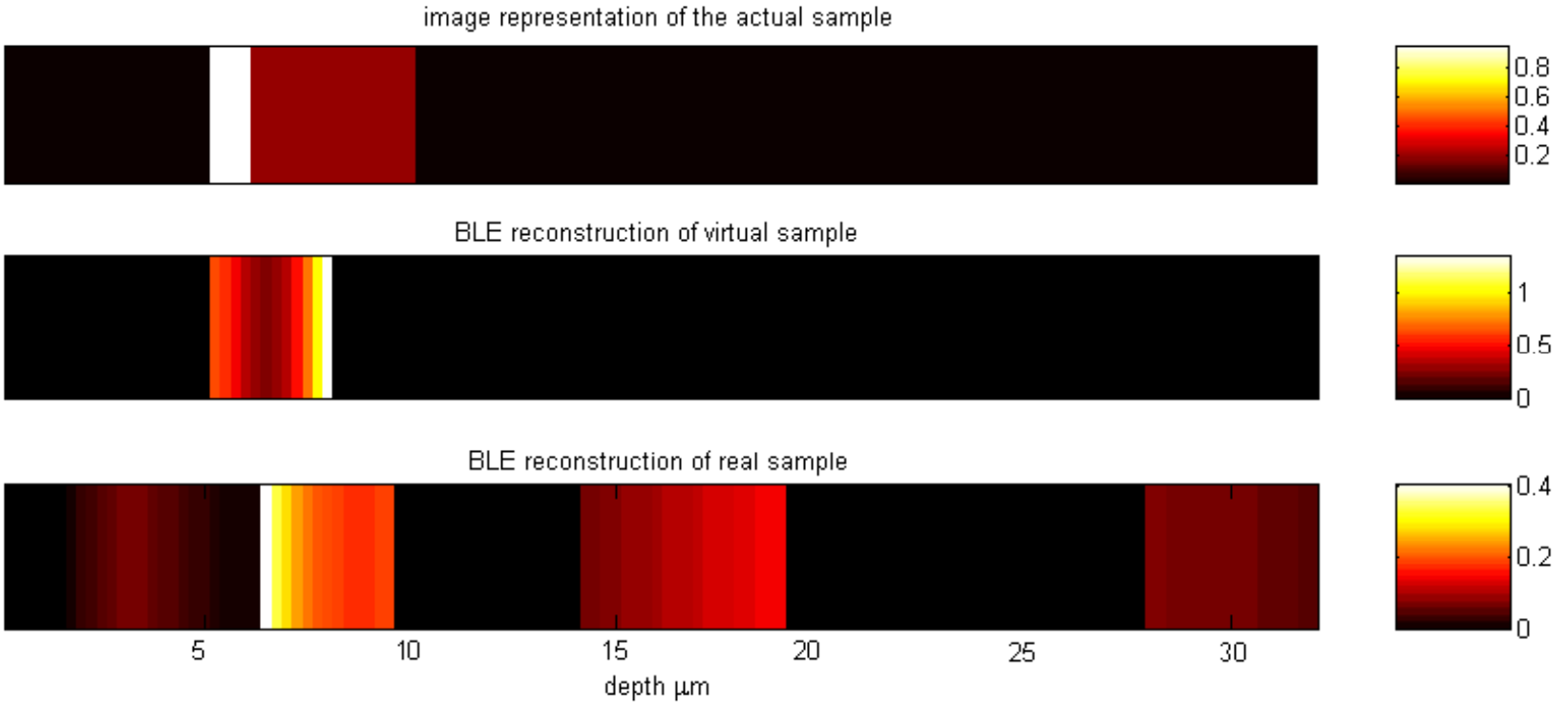
image representation of the actual sample
0.8
0.6
0.4
0.2
BLE reconstruction of virtual sample
1
0.5
0
BLE reconstruction of real sample
0.4
0.2
0
5
10
15
20
25
30
depth µm

Figure 9

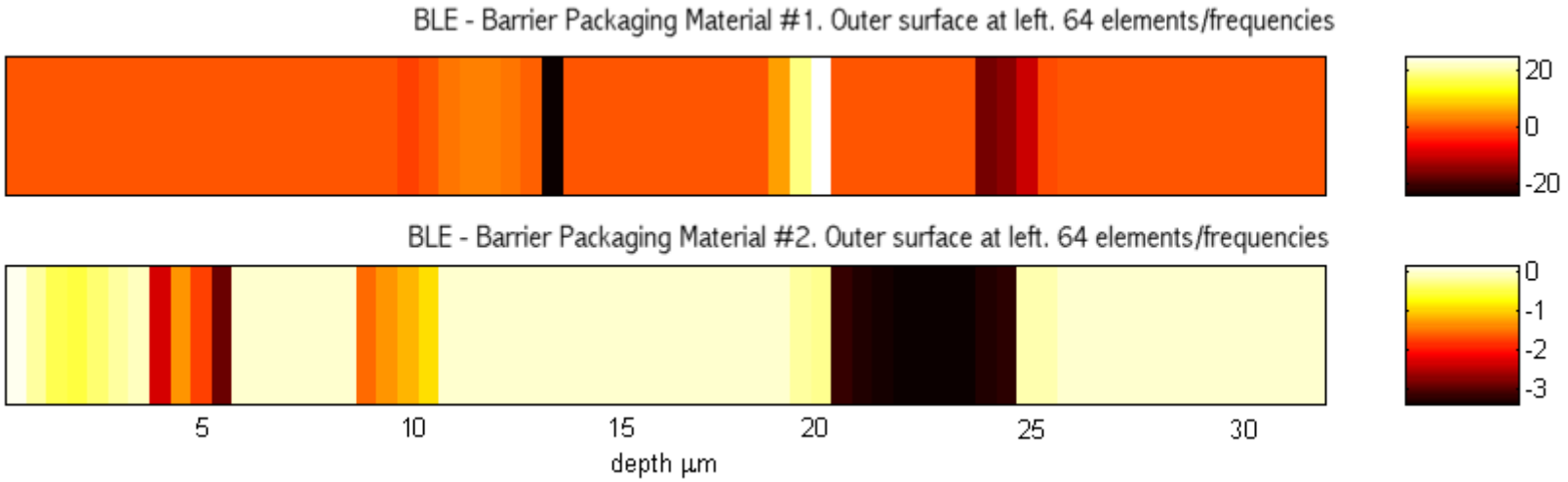
BLE - Barrier Packaging Material #1. Outer surface at left. 64 elements/frequencies
20
0
-20
BLE - Barrier Packaging Material #2. Outer surface at left. 64 elements/frequencies
0
-1
-2
-3
5
10
15
20
25
30
depth µm

Figure 10

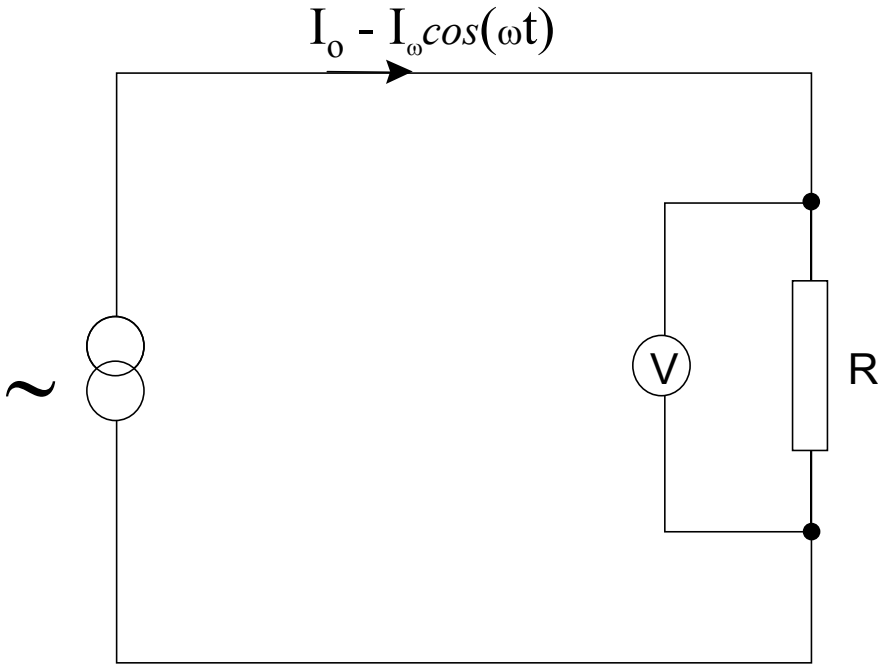
$I_o - I_\omega cos(\omega t)$
~
V
R